



Published in final edited form as:

Neuroimage. 2011 July 15; 57(2): 526–538. doi:10.1016/j.neuroimage.2011.04.002.

Mapping Cortical Representations of the Rodent Forepaw and Hindpaw with BOLD fMRI Reveals Two Spatial Boundaries

Artem G. Goloshevsky^{1,2}, Carolyn W.-H. Wu^{1,3}, Stephen J. Dodd¹, and Alan P. Koretsky¹

¹National Institute of Neurological Disorders and Stroke, National Institutes of Health, Bethesda, MD, USA

Abstract

Electrical stimulation of the rat forepaw and hindpaw was employed to study the spatial distribution of BOLD fMRI. Averaging of multiple fMRI sessions significantly improved the spatial stability of the BOLD signal and enabled quantitative determination of the boundaries of the BOLD fMRI maps. The averaged BOLD fMRI signal was distributed unevenly over the extent of the map and the data at the boundaries could be modeled with major and minor spatial components. Comparison of three-dimensional echo-planar imaging (EPI) fMRI at isotropic 300 μm resolution demonstrated that the border locations of the major spatial component of BOLD signal did not overlap between the forepaw and hindpaw maps. Interestingly, the border positions of the minor BOLD fMRI spatial components extended significantly into neighboring representations. Similar results were found for cerebral blood volume (CBV) weighted fMRI obtained using iron oxide particles, suggesting that the minor spatial components may not be due to vascular mislocalization typically associated with BOLD fMRI. Comparison of the BOLD fMRI maps of the forepaw and hindpaw to histological determination of these representations using cytochrome oxidase (CO) staining demonstrated that the major spatial component of the BOLD fMRI activation maps accurately localizes the borders. Finally, 2–3 weeks following peripheral nerve denervation, cortical reorganization/plasticity at the boundaries of somatosensory limb representations in adult rat brain was studied. Denervation of the hindpaw caused a growth in the major component of forepaw representation into the adjacent border of hindpaw representation, such that fitting to two components no longer led to a better fit as compared to using one major component. The border of the representation after plasticity was the same as the border of its minor component in the absence of any plasticity. It is possible that the minor components represent either vascular effects that extend from the real neuronal representations or the neuronal communication between neighboring regions. Either way the results will be useful for studying mechanisms of plasticity that cause alterations in the boundaries of neuronal representations.

Published by Elsevier Inc.

Address Correspondence to: Alan P. Koretsky, LFMI, NINDS, Building 10, Rm B1D728, 10 Center Drive, Bethesda, MD, 20892, koretskya@ninds.nih.gov.

²Present address: Bruker BioSpin Corp., Billerica, MA, USA

³Present address: Unit of Brain Plasticity, Laboratory of Integrated Biology, NeuroSpin (CEA), Gif-sur-Yvette, France

Publisher's Disclaimer: This is a PDF file of an unedited manuscript that has been accepted for publication. As a service to our customers we are providing this early version of the manuscript. The manuscript will undergo copyediting, typesetting, and review of the resulting proof before it is published in its final citable form. Please note that during the production process errors may be discovered which could affect the content, and all legal disclaimers that apply to the journal pertain.

Keywords

BOLD; CBV; fMRI; rat; electrical stimulation; cortical representation; induced cortical plasticity; peripheral denervation; histochemical staining

1. Introduction

Blood oxygenation level-dependent functional magnetic resonance imaging (BOLD fMRI) is a non-invasive, *in vivo* technique widely used for mapping of the brain function in humans and animals (Huettel et al., 2004). There have been a number of comprehensive studies focused on the relationship between the hemodynamic components constituting the BOLD signal and neuronal function (Lauritzen, 2005; Logothetis, 2002; Smith et al., 2002; Ureshi et al., 2004; Stefanovic et al., 2006). It is clear that in most normal situations there are strong correlations between measures of neuronal activity and the amplitude of the BOLD signal. There have been fewer studies of the spatial relationship between the topography of the BOLD activation maps and the sites of neuronal activation (Engel et al., 1997; Kim et al., 2004; Shmuel et al., 2007; Kim and Fukuda, 2008).

Much attention has been given to whether or not BOLD fMRI can detect cortical columns and which of BOLD, perfusion, or cerebral blood volume weighted fMRI localize best (Kim et al., 2000; Duong et al., 2000; Fukuda et al., 2006; Jin et al., 2008). Furthermore there have been a number of studies measuring the point - spread function of BOLD fMRI activation maps (Park et al., 2004; Parkers et al., 2005; Shmuel et al., 2007). These studies typically make two assumptions that have not been well examined in the context of fMRI. First, they assume that the neuronal representation is spatially well defined. Indeed, it is well known from neurophysiological studies that neuronal representations are not precisely defined by the underlying anatomy (Chapin and Lin, 1984; Chapin et al., 1987). Even at the level of well-defined anatomical columns there is a spill-over in much weaker and diffused neuronal activity to neighboring columns (Tucker and Katz, 2003; Ajima and Tanaka, 2006). Furthermore, there is evidence that there is reciprocal neuronal communication even between boundaries of large neuronal representations (Berwick et al., 2004). The second assumption is that the statistical thresholds usually used define the significant areas of activation and that these are relevant as the borders of the representation. There have been a few studies that have addressed how BOLD fMRI activation maps are affected in individuals with signal averaging, and in these cases increase in signal to noise has led to the notion that BOLD fMRI maps will increase with increasing signal to noise (Huettel and McCarthy, 2001; Saad et al., 2003). However, even with averaging that is feasible in humans the number of activated voxels depends critically on the statistical threshold. One estimate is that it would take more than 150 single trials to detect all active voxels and reliably determine the global spatial extent of the activation (Huettel and McCarthy, 2001).

In the present work, the well-established model of electrical stimulation of a rat limb (Bock et al., 1998; Palmer et al., 1999; Spenger et al., 2000; Chen and Shen, 2006) was used to study how data averaging influences the spatial distribution of the BOLD signal magnitude across the extent of detectable activation area. Particular attention was paid to the improvements of the certainty of BOLD signal definition at the boundaries of the adjacent

representations after data averaging. Very high-resolution fMRI obtained at 11.7 T and utilizing either multi-slice pulse sequences with 150 μm in-plane resolution or three-dimensional sequences with 300 μm isotropic resolution were used to define the resulting activation maps. This data was used to determine the effects of averaging electrical stimulations, to quantitatively determine the spatial localization of the fMRI maps' boundaries, and to compare the spatial extent of the boundaries of the neighboring hindpaw and forepaw cortical representations with each other and with cytochrome oxidase based histology. The results indicate that a reasonable number of about forty blocks of thirty seconds stimulation periods was sufficient to lead to a stable spatial BOLD fMRI signal. Interestingly, at the high signal to noise ratio obtained, two spatial components could be defined at the boundary of the BOLD fMRI data maps. There was a major component, whose spatial extent did not extend into neighboring regions and agreed well with the histologically determined borders of the hindpaw or forepaw representations. There was also a minor component which was about 30% in amplitude that extended well into the neighboring representation either defined by the major fMRI component or by histology. Similar results were obtained with cerebral blood volume (CBV) based fMRI using iron oxide particles as contrast agent, indicating that the presence and extent of the minor component borders might not be due to vascular artifacts potentially associated with BOLD fMRI. With the the three-dimensional BOLD fMRI changes in the boundaries of somatosensory maps (cortical reorganization) following peripheral nerve deafferentiation could be measured and should enable better quantitation of changes during plasticity over a number of cortical areas (Dawson and Killackey, 1987; Karni et al., 1995; Melzer and Smith, 1998; Calford, 2002, Yu et al., 2010). Denervation of the hindpaw led to an increase of the extent of the adjacent major component of the forepaw representation. Interestingly, one major spatial component was sufficient to fit the border of the fMRI representation after plasticity and the extent of growth was not significantly different from the boundary value of the minor component in the areas that had not undergone plasticity. Better quantitation of the spatial extent of fMRI should enable interesting questions about the spatial extent of BOLD fMRI under a variety of stimulation paradigms to be addressed (Godde et al., 1996; Ogawa et al., 2000; Berwick et al., 2004).

2. Methods

2. 1. Animal preparation

All experiments were performed in compliance with guidelines set by the National Institutes of Neurological Disorders and Stroke ACUC. Fifteen male Sprague-Dawley rats (200–300 g) were anesthetized with isoflurane (5% induction, 1.5% maintenance) and orally intubated for artificial mechanical ventilation. Catheters were placed into the femoral artery and vein for arterial blood pressure monitoring, sampling of blood gases and drug delivery. Isoflurane was discontinued and anesthesia was switched to α -chloralose using 80 mg/kg initially, and then followed by a continuous infusion of 26.7 mg/kg/hr. The animals were placed into a stereotaxic head holder with ear and bite bars. An intravenous injection of pancuronium bromide (4 mg/kg) was given once per hour to prevent motion. Expired CO_2 , rectal temperature and blood pressure were continuously monitored. Blood gases were measured and maintained at normal levels. For CBV fMRI studies five rats were given 20 mg Fe/kg

i.v. using 30 nm dextran coated iron oxide particles (Molday IONTM, BioPAL, Worcester, MA). Iron oxide was given five minutes before the commencement of CBV weighted fMRI. For the study of the functional cortical reorganization, six adult rats underwent an excision of the sciatic and saphenous nerves in a single hindpaw as previously described (Pelled et al., 2007), and BOLD fMRI measurements were conducted in the following 2–3 weeks.

2.2. Stimulation paradigm

Two needle electrodes were subcutaneously inserted into a forepaw and/or a unilateral hindpaw when needed. The limbs were stimulated by application of trains of rectangular pulses of 330 μ s duration at a repetition rate of 3 Hz supplied with a World Precision Instruments stimulator (WPI, Sarasota, FL). Maximum current amplitude was 2.5 mA in all stimulations. The fMRI block design was utilized for stimulation and the paradigm of a single fMRI session consisted of five blocks (200 MRI scans). Each block employed 30 s of stimulation, which contained 90 stimulation pulses and 20 MRI scans, bordered by 15 s rest periods, which consisted of 10 MRI scans. Representative time courses of the stimulation and the corresponding evoked BOLD signal during one fMRI session are shown in Fig. 1A. Data is shown as a function of the number of averaged sessions used.

2.3. Functional Magnetic Resonance Imaging experiments

Functional MRI experiments were performed with an 11.7 T/31 cm magnet (Magnex Scientific, Ltd., Abington, UK) interfaced to a Biospec-Avance console (Bruker-Biospin, Corp, Billerica, MA) and equipped with a 9 cm ID gradient set (Resonance Research, Billerica, MA). FASTMAP was employed for shimming (Gruetter, 1993). A laboratory-built, 2 cm receive-only surface coil was used inside a 7 cm ID transmit-only coil. The imaging experiments were divided into two groups:

The first group of experiments (5 animals) utilized a multi-slice, spin-echo single-shot EPI sequence. FOV was 1.92 \times 1.92 cm² with a 128 \times 128 matrix leading to a nominal in-plane resolution of 150 μ m. The bandwidth was 400 kHz, TE was 45.5 ms and TR was 1.5 s. Five 1 mm thick slices were acquired, covering the forebrain and middle brain. Sessions of forepaw stimulation were collected as long as an animal was in normal physiological condition. The duration of studies varied from 5 to 7 hours (44 sessions was the most performed).

The second group of experiments (5 animals for BOLD fMRI and 5 animals for CBV fMRI) utilized a 3D gradient-echo single-shot EPI sequence. FOV was 1.92 \times 1.92 \times 0.96 cm³ with a 64 \times 64 \times 32 matrix leading to a nominal, isotropic resolution of 300 μ m. The bandwidth was 200 kHz, TE was 13.22 ms and TR was 46.875 ms. The right forepaw and hindpaw were stimulated in separate sessions. A total of 26 sessions were collected for each animal; 13 for each limb.

The third group of experiments (6 animals for BOLD fMRI study of cortical plasticity) also utilized the same 3D EPI sequence as described above, however both forepaws were simultaneously stimulated and at least 13 sessions were collected for each animal.

2.4. Data Analysis

Upon completion of the collection of fMRI sessions, images were averaged on voxel by voxel basis. Figure 1 and Figure 2 indicate the steps taken. Fig. 1B shows a high-resolution anatomical EPI image obtained with averaging of thirty-three fMRI sessions from a single animal. The plot in Fig. 1C shows a signal magnitude profile of the averaged image, as well as the image profiles of the single sessions used for averaging. All the magnitude profiles correspond to the same ROIs represented by the blue line across the edge of the cortex shown in Fig. 1B. Motion of animals was minimal due to the ear and bite bars used to hold the head and the regular injections of pancuronium bromide, therefore, no additional processing to correct for motion was employed. The averaged data was then used to calculate the t-maps of BOLD signal ($p < 0.05$) in units of percent signal change. Only groups of at least 4 activated pixels were taken into consideration. STIMULATE software was used for the calculation of maps (Strupp, 1996).

Fig. 2A shows an averaged fMRI activation map of the forepaw representation overlaid upon an averaged anatomical image. Twenty fMRI sessions, obtained in the first group of experiments with a resolution of $150\ \mu\text{m}$, were averaged for the map and the image shown. The map profiles of the BOLD signal were manually selected for subsequent analysis as demonstrated in Fig. 2A with the blue ROI line. ImageJ software (National Institutes of Health, USA) was used to select the profiles. The ROIs were drawn in the same fashion for all the animals: from the midline of the brain along the cortical layers IV and V ($600\text{--}1000\ \mu\text{m}$ below the pial surface) in the coronal orientation. Two to three profiles corresponding to the same selection line shifted across layers IV and V were averaged for the final profile representation of each map. Fig. 2B shows a map profile corresponding to the ROI selection of the Fig 2A. The abscissa values of the length along the ROI are counted from the midline of the brain. It is worth noting that the threshold introduced upon the raw averaged functional data by application of the t-test did not influence the features of signal distribution at the boundaries of the BOLD activation maps (Fig. 2B).

The dependence of the shape delineation of the BOLD signal profile upon the number of fMRI sessions used for averaging was investigated in a way similar to the technique reported in Huettel and McCarthy, 2001. Four series of 15 averages of sampled fMRI sessions, varying in the number of sessions combined (for 3, 5, 8 and 15 averages), were computed. While averaging, fMRI sessions were randomly sampled out of the total number of repeated experiments. Then the activation t-maps were calculated for each of the averages in the series and the profiles were selected based on the same ROI line. The standard deviation of the BOLD signal across each series of averages was calculated at the same data point of the profile signal fall-off corresponding to the border of the activation map.

The linear ROI selection lines were drawn in a different fashion for the comparison of the denervated side of the cortex to the control side (Fig. 8A). The 3D data sets were axial-oriented and the equal left and right sides of the ROIs formed an isosceles triangle with its top placed into the midline between the hemispheres. One axial slice which most favorably represented both forepaw and hindpaw representations was used to collect the ROI profiles data for averaging across the six animals (the same slice for all of the animals).

2.5. Defining the boundaries of the spatial extent of fMRI

For normal control animals the shapes of the fMRI activation map signal profiles were roughly symmetrical around their maxima. The appearance of the spatial features of the signal profile boundaries was similar in the medial and lateral directions (i.e. hindpaw and orofacial representations respectively). As shown in Fig. 3A and 3B, the shape of the border of either half of the BOLD signal profile could be well modeled by a combination of two parabolic-shaped curves as expressed by the equation

$$F_4 = F_1 + F_3, \quad (1)$$

where

$$F_1 = \begin{cases} F_0, & F_0 \geq 0 \\ 0, & F_0 < 0 \end{cases} \quad (2)$$

with

$$F_0 = -a_0(x - a_1)^2 + a_2 \quad (3)$$

and

$$F_3 = \begin{cases} F_2, & F_2 \geq 0 \\ 0, & F_2 < 0 \end{cases} \quad (4)$$

with

$$F_2 = -a_3(x - a_4)^2 + a_5. \quad (5)$$

The activation profiles were normalized by the values of their maximum signal and then fitted by the expression (1) using the variables a_i ($i = [0, 5]$) as parameters of the fit. Then, the profiles' borders were further characterized by the points where the curves F_1 and F_3 crossed the abscissa (Fig. 3B). Using results of the best fit, the cross-section points were calculated as

$$zero_{major} = -\sqrt{\frac{a_2}{a_0}} + a_1 \quad (6)$$

and

$$zero_{min.or} = -\sqrt{\frac{a_5}{a_3}} + a_4. \quad (7)$$

2.6. Histology

A separate group of four rats was used for histological stain to reveal the forepaw and hindpaw anatomical somatosensory representations in the cortex. A histochemical stain for the mitochondrial enzyme cytochrome oxidase (CO) was used. Density of the CO stain in the cortical layer IV reflects density of the aggregates of granule cells (neuronal density) and thus cytoarchitectonically delineates regions of sensory representations (Wong-Riley and Welt, 1980; Land and Simons, 1985; Hevner et al., 1995).

Histochemically stained coronal sections (40 μm thick) were considered from the region of the brain located between 0.35 and 0.85 mm posterior to the bregma. The intensity of staining (relative lightness/darkness of color) was visually inspected with regard to the borders of the forepaw and hindpaw representations, and the photoimages (Leica-Vashaw Scientific, Inc., Norcross, GA) of sections were manually marked with lines representing histological borders. Then the ROI selection lines were drawn on the marked photoimages in the same manner as it was done for the fMRI representations: from the midline of the brain along the layer IV. The abscissa values of the length along this ROI selection line corresponding to its cross-section points with the visually scored border marks were recorded as the histological border values. The fMRI activation maps corresponding to a single coronal slice at the same location in the brain were selected from the 3D data sets (0.3 mm isotropic resolution) and the shapes of their signal profiles were analyzed at the borders as discussed above for comparison of the boundaries of the fMRI maps of the cortical representations and the histology. No attempt was made to adjust for shrinkage that may have occurred due to fixation, sectioning and staining of the sections.

3. Results

3.1. Averaging of high-resolution fMRI activation maps enables quantification of boundaries

As demonstrated in Fig. 1, the averaging of fMRI sessions improves the signal-to-noise ratio and sharpens the contrast of the anatomical high-resolution EPI data, thus enabling the more precise analysis of the derived functional maps. Fig. 2A and Fig. 2B show that to avoid contamination with signals from the draining vein at the surface of the cortex, the ROI selection of the activation signal profiles is performed at the deeper cortical layers. The shape of the BOLD fMRI signal profile depends on the number of fMRI sessions used for averaging. Fig. 2C and 2D show two sets of the activation map profiles; the set in Fig. 2C corresponds to a series of 15 randomly sampled single fMRI sessions. The other set in Fig. 2D corresponds to a series of 15 averages of 8 randomly sampled fMRI sessions. The profiles are from the same ROI selection defined by the blue line in Fig. 2A. It can be seen that the stability of the profile shape increases as more fMRI sessions are averaged. The plot of the standard deviation of the BOLD signal at the profile border versus the number of averaged sessions is shown in Fig. 2E. This data indicated that by eight or more averaged sessions the shape of the map profile shows little variation even if the averaging is increased. This suggests that the minimum number of averages should be eight sessions with the parameters used in this study and increasing the number of averages further has only minor effects on the delineation of the activation map borders.

From the representative activation map and its signal profile shown in Fig. 2A and 2B it can be seen that areas of lower BOLD signal intensity bordered the area of greater BOLD signal. As demonstrated in Fig. 3C, this was consistently observed for all animals used in the high-resolution experiments. To evaluate the distribution of the BOLD signal at the boundary of the representation, the activation profiles were further studied by fitting the spatial extent of the curves. It is clear from the data that at least two spatial components were required to fit the data. The position of the boundary of each component was quantitated by the parameters $zero_{major}$ and $zero_{minor}$ as determined by the fit of equations (6) and (7) to the data. Table 1 summarizes the results of the fit for five animals from the forepaw representation. The averaged major component boundary, $zero_{major}$, was at the distance of $2485 \pm 134 \mu\text{m}$ from the midline of the brain along the cortex. The boundary of the minor component, $zero_{minor}$, was at $1709 \pm 400 \mu\text{m}$ from the midline of the brain. This difference between $zero_{major}$ and $zero_{minor}$ was statistically significant ($p < 0.05$). Fig. 3D shows the boundary of the BOLD signal profile in the medial direction and the border positions of the two components averaged over five animals.

3.2. Three-dimensional BOLD and CBV fMRI activation maps enables comparison of boundaries between forepaw and hindpaw representations

Fig. 4A shows representative averaged BOLD activation maps of forepaw and hindpaw overlaid upon averaged anatomical images in the axial orientation obtained from the 3D MRI. It can be seen that, due to draining veins, the BOLD signal deeper in the cortex is localized much better than on the surface consistent with the two-dimensional maps (Fig. 2A) and previous studies (Keilholz et al., 2006; Goloshevsky et al., 2008). Fig. 4B shows BOLD signal profiles from the activation maps of forepaw and hindpaw corresponding to the same ROI (the blue selection line in Fig. 4A). The intensity of the hindpaw BOLD activation was lower than that of the forepaw. It was previously demonstrated that due to a lower sensitivity of the hindpaw, higher electrical currents were needed to induce similar fMRI activation of the same amplitude as in the forepaw (Bock et al., 1998). Here, the same amplitude of the electrical current was used for the stimulation of both the forepaw and hindpaw, since signal to noise was good enough for reliable determination of $zero_{major}$ and $zero_{minor}$ for both representations.

The overlap between the fMRI maps of forepaw and hindpaw representations (Fig. 5A) was investigated by the analysis of the map profiles at their boundaries. Fig. 5B shows representative BOLD signal profiles separately obtained for the forepaw and hindpaw from the same animal and corresponding to the same ROI as indicated by the blue selection line in Fig. 5A. The activation profiles from all animals demonstrated a significant overlap between the representations and this was further studied by the analysis of the spatial border positions where BOLD signal went to zero for the two major spatial components in each representation (Fig. 5B). The $zero_{major}$ and $zero_{minor}$ values, described by the equations (6) and (7), were used to quantify the features of the profile shapes at the adjacent boundaries for both forepaw and hindpaw. Table 2 summarizes the values of the fit for five animals. The border value $zero_{major}$ of the major component of the forepaw representation on its hindpaw side was $2435 \pm 289 \mu\text{m}$ from the brain midline, which was not significantly different from the value obtained from the two-dimensional fMRI data reported above. The

border value $zero_{major}$ of the major component of the hindpaw representation was at $2587 \pm 310 \mu\text{m}$ from the midline. The boundary positions for these two major components were not statistically different indicating that fMRI at the resolutions used could not detect a significant separation between the two major representations.

The values of border position $zero_{minor}$ for both minor components from the hindpaw and forepaw representations were significantly different from the $zero_{major}$ values (Table 2). For the forepaw there was good agreement for the $zero_{minor}$ value obtained from the 2D and 3D fMRI data. Interestingly, $zero_{minor}$ border positions of the minor components extended well into the neighboring representation. The forepaw $zero_{minor}$ values at $1463 \pm 289 \mu\text{m}$ from the midline was significantly ($p < 0.05$) closer to the midline than the hindpaw $zero_{major}$ ($2587 \pm 310 \mu\text{m}$) indicating that the forepaw minor $zero_{minor}$ boundary was inside the hindpaw $zero_{major}$ boundary. Similarly the hindpaw minor $zero_{minor}$ boundary was at $3334 \pm 235 \mu\text{m}$ which was significantly further ($p < 0.05$) than the forepaw $zero_{major}$ boundary on the hindpaw side at $2435 \pm 289 \mu\text{m}$ from the brain midline. Fig. 5C shows the BOLD signal profile and the values of the adjacent boundaries for the forepaw and hindpaw fMRI representations averaged for five animals. Thus, the overlap detected in the typically thresholded BOLD fMRI maps would not be due to overlap of the major BOLD fMRI spatial components but due to the extension of the minor components into the territory defined by the major components.

There is general consensus that BOLD fMRI can give rise to vascular artifacts. The use of spin-echo EPI at high field reduces these artifacts (Uludag et al., 2009), but they can still contribute as demonstrated by the draining vein detected in the present and earlier works performing fMRI on the rodent forepaw representation (Keilholz et al., 2006; Goloshesky et al., 2008). This opens the possibility that the minor components we detected at the boundaries are due to vascular artifacts. Care was taken to analyze the BOLD fMRI data from deeper cortical regions to avoid the obvious surface vessel artifacts; however, vascular artifacts in BOLD fMRI from penetrating venules remained a possibility. There is some evidence that CBV weighted, iron-oxide fMRI reduces the possibility for vascular artifacts (Mandeville et al., 1998; Keilholz et al., 2006; Zhao et al., 2006). Therefore, 3D CBV fMRI maps of forepaw and hindpaw representations were obtained to determine if there were major and minor spatial components as found with BOLD fMRI. Fig. 6 shows data obtained with CBV based fMRI. The CBV activation maps were investigated in the coronal orientation as shown in Fig 5A and the fit of the boundaries of the CBV signal profiles is shown in Fig. 6B. Table 3 summarizes the results of the fit for five animals. The CBV fMRI analysis also demonstrated two spatial components at the same border locations as the BOLD fMRI data.

To test whether the fMRI defined major component borders of the somatosensory representations agreed with the anatomical borders, histology was quantified in a manner similar to the fMRI data. As described above, the histological borders between the sensory cortical representations of forepaw and hindpaw were quantified by means of the ROI analysis of the visually scored photoimages of the CO-stained brain slices at approximately the position of layer IV. The border values obtained from histology are summarized in Table 4. As an example of quantitative comparison between the histology and the fMRI data, the

histologically defined border of the hindpaw between the forepaw and hindpaw representations at $2542 \pm 58 \mu\text{m}$ was not significantly different from both of the $zero_{major}$ value for the 3D CBV fMRI forepaw representation at $2765 \pm 292 \mu\text{m}$ and the $zero_{major}$ value for the 3D CBV fMRI hindpaw representation at $2720 \pm 136 \mu\text{m}$. The histologically defined border of the forepaw at $2887 \pm 37 \mu\text{m}$ was not significantly different from either of the 3D CBV fMRI border values as well. Indeed, these values all agree within one pixel of 300-micron resolution of the fMRI data. Thus, there is excellent agreement between the major component boundary defined by the fMRI and the anatomical boundary defined by CO staining. Based on the observed correlation between the histology and fMRI, a strong spatial correspondence can be proposed between the areas of higher signal in the fMRI activation maps and the somatosensory cytoarchitectural representations. The $zero_{minor}$ boundary values of the forepaw and hindpaw minor components (1797 ± 490 and $4146 \pm 797 \mu\text{m}$ from the brain mid-line) obtained from the fMRI data were statistically different from the histological borders again demonstrating that the minor components extend into the neighboring representation.

3.3. Assessment of functional cortical plasticity with BOLD fMRI mapping of adjacent somatosensory representations

Fig. 8A shows averaged BOLD activation maps of bilateral forepaw representations overlaid upon the anatomical EPI images in the axial orientation (2 slices shown). The left hemisphere in the images corresponds to the denervated hindpaw. Therefore the isosceles sides of the blue selection line represent the forepaw of the altered representation (left) and the control forepaw (right) correspondingly. The ROI profiles from an individual rat shown in Fig. 8B demonstrate the comparison between the appearances of representation borders for the normal/control forepaw and for the forepaw of the reorganized representation. The position of the profiles in these animals is in a different plane than used in the previous set of experiments since data shown is from an axial orientation. The growth of the reorganized fMRI forepaw representation into the representation of the denervated hindpaw can be readily detected. This growth would translate into an increased number of pixels above threshold as it would be typically quantified to measure changes in representations with fMRI. Fig 8C shows the average profiles from all six animals. There is some indication of the lateral expansion in the forepaw map boundaries, which was primarily due to the normalization and averaging of the fMRI signal profiles (there were differences in brain sizes of individual rats, ROIs asymmetry due to the slightly angled position of the brain in the imaging slice and also differences in the magnitude of stimulation for left and right forepaws due to the slightly different positioning of the electrodes). The lateral expansion was not observed consistently for all of the individual rats in the group (as can be seen in the Figure 8A corresponding to a single animal). The boxes indicate the location of the 50% intensity point for control (blue box) and denervated (red box). The box size represents mean \pm one standard deviation.

Fig. 8D shows the results of the fitting of forepaw representation for both control (black line) and denervated animals (red line) at the border with the hindpaw representation. In control animals a two component analysis fit the data best. However, the boundary of the reorganized forepaw was best fitted by the major component only. A two component fit

would either not converge, had a poor quality of fit, or had a very small minor component (data not shown). Interestingly, the border position $zero_{major}$ (red box) in the expanded reorganized area overlaps with the border position $zero_{minor}$ (blue box) of the control forepaw (Fig. 8D). To illustrate how these forepaw boundary positions fall in relation to the hindpaw boundaries, the control and denervated profiles are mapped with the control hindpaw representation in Fig 8E (grey boxes). Positions of all borders of the major and minor components from control rats and the border position of the major component of the forepaw representation from hindpaw denervated rats are summarized in Table 5.

4. Discussion

The goal of the present work was to determine if high sensitivity and high-resolution BOLD fMRI could lead to a quantitative determination of the boundaries of the cortical representations of the rat forepaw and hindpaw. The data indicate that there are large increases in the signal to noise of spin-echo BOLD fMRI maps obtained at 11.7T at the high resolution when up to about 8–10 fMRI sessions are used for signal averaging. Increases after this are much smaller. The relation between the number of stimulations and improvement in signal to noise will be very dependent on the precise imaging conditions used due to well-studied issues of the noise properties of the BOLD signal, such as whether physiological or MRI system noise dominate (Thomas et al., 2002). It has been previously shown that signal averaging improves the SNR of the fMRI signal from the human brain, and under certain conditions this can lead to an increase of the spatial extent of pixels that get above statistical activation threshold and thus an apparent increase in the size of the activation (Huettel and McCarthy, 2001; Saad et al., 2003). Furthermore, it was demonstrated that even after a large number of averages there was still evidence that many activated voxels remained below the threshold (Saad et al., 2003). These results open the question of how to quantify the borders of fMRI activations especially when plasticity changes these borders (Yu et al., 2010).

In the rat somatosensory cortex signal averaging leads to a stabilization of the activation area indicating that the borders can be clearly defined. Unexpectedly, it was found that the magnitude of the BOLD fMRI activation maps at their boundaries was not well described with a single spatial component. The profiles of the BOLD signal obtained from mid-cortical layers across the activation area demonstrated peripheral areas of reduced BOLD signal surrounding a central region of greater activation. The larger central activation, surrounded by a weaker activation was consistently observed for a number of animals. Therefore, quantitatively defining the boundaries by using curve fitting of the signal intensity distributions vs. spatial extent of the BOLD fMRI data required fitting to two components: a major component and a minor component that was about 30 % as large in amplitude as the major component. Previously, this approach of extrapolating fMRI data to a border was used but without fitting second minor component (Yu et al., 2010). In this previous work there was significant overlap in representations. In the present work, the border positions of where the major component of the fMRI signal went to zero did not overlap for the cortical forepaw and hindpaw representations. Therefore, removing the minor spatial component led to separation of the major fMRI components. The cytoarchitectonic divisions within the rat somatosensory cortex are well known and their

detailed maps have been previously obtained using microelectrode recordings (Chapin and Lin, 1984) and histochemical staining (Land and Simons, 1985; Dawson and Killackey, 1987). Specifically, it has been shown that the granular zones (dense aggregates of layer IV granular cells) of the hindpaw and forepaw do not overlap and there is a spacer of less granular cortex (perigranular zone) between them. The positions of the boundaries of the major BOLD fMRI components agreed well with histological data for the anatomical boundaries between the forepaw and hindpaw granular zones. This agreement suggests that the border of the major spatial component of a functional BOLD map accurately localizes the cytoarchitectural boundaries. A significant drawback to fitting the fMRI data to two spatial border components is that excellent signal to noise achieved with averaging many stimulations needed to be obtained.

The correspondence of the boundaries of BOLD fMRI representations and histological borders was excellent despite a number of factors that complicated the comparison. The fixation and sectioning of the brain can distort the brain slices and it is well known that the EPI sequence can cause geometrical distortions (Chen et al., 2006). Finally, the thicknesses of the histological and MRI slices were quite different. Nevertheless, there was a good agreement between the fMRI localization of the boundary values $zero_{major}$ of the forepaw and hindpaw major components and the histological determination of the boundaries. Therefore, it can be proposed that the boundaries of major signal in the BOLD activation maps are strongly related to the boundaries between the cytoarchitectural somatosensory representations. There is emerging evidence from manganese enhanced MRI (Silva et al., 2008), from T₁ weighted MRI (Barbier et al., 2002; Bock et al., 2009), and from new phase contrast susceptibility weighted MRI techniques (Duyn et al., 2007) that cytoarchitectural information can be obtained from MRI. This opens the possibility of getting both functional and anatomical information from the same subject using the same MRI sequences and thus enabling an even more quantitative comparison of borders. Comparison of fMRI to statistically generated anatomical borders has been performed in humans (Hinds et al., 2009; Yeo et al., 2010). However, variability in both the functional and anatomical borders does not yet allow detailed comparison.

There has been much interest in what are the limits of fMRI for resolving neuronal representations. There is mounting evidence that fMRI can detect columnar and laminar activity (Kim et al., 2000; Duong et al., 2001; Silva and Koretsky, 2002; Zhao et al., 2006; Fukuda et al., 2006; Koopmans et al., 2010; Polimeni et al., 2010). To help quantify this issue of the ultimate resolution of fMRI, several techniques have been proposed to measure the point spread function for fMRI using the border between neuronal representations (Engel et al., 1997; Park et al., 2004; Parkers et al., 2005; Shmuel et al., 2007). Recently, high resolution BOLD fMRI data from the human and cat brain has put an upper limit to the point spread function of 1.6 mm using gradient echo EPI (Park et al., 2004; Shmuel et al., 2007) and a low limit of 400–500 microns in cat visual cortex (Duong et al., 2001). When using the mid-points of the major components found in this study for the activation maps of forepaw and hindpaw, determination of a point spread function gives values from 0.2 to 1.2 mm across five animals (0.7 mm on average). However, analysis of the mid-points does not make full use of the quantitative data obtained for the boundaries in the present study.

Asking questions about the precise localization of boundaries of fMRI activation is another way of addressing the issue of how precisely fMRI can map neuronal representations. In the high resolution 2D data the boundary of the major component was determined with precision comparable to the pixel resolution, thus indicating that the localization of this boundary was on the order of the 150 μm pixel resolution. Indeed, further evidence that the border of the major component of BOLD fMRI can localize activity within the somatosensory cortex very precisely is that the forepaw and hindpaw representations agreed to within a pixel of 300 μm . Finally, the histological boundaries between the forepaw and hindpaw are separated by a dysgranular zone, which is about 100 to 300 μm . Under the conditions used, there was no evidence of the dysgranular zone, because the localizations of the boundaries between the forepaw and the hindpaw fMRI representations were not significantly different. This indicated that either BOLD fMRI cannot detect features this small or that higher resolution data is required to identify this feature.

Unexpectedly, in addition to the major component of the fMRI data there were also minor components, which extended well into the neighboring representations. The forepaw minor component extended about 50% of the way into the hindpaw and the hindpaw minor component extended about 30% of the way into the forepaw representation. This is consistent with previous work where significant overlap between the forepaw and hindpaw representations has been consistently observed in the fMRI mapping studies (Bock et al., 1998; Palmer et al., 1999; Spenger et al., 2000; Chen and Shen, 2006; Yu et al., 2010). Based on the present work it is the minor components of the fMRI signal that are responsible for this overlap in regions. Thus, care must be taken to separate out the borders of these two spatial components if any conclusions about the position of fMRI borders are to be made.

The significance and the origins of the minor components of the BOLD fMRI signal are not clear. Indeed, a major remaining question is whether they are caused by underlying neuronal activity or by vascular effects. When using BOLD fMRI one must always be concerned about artifacts due to vascular effects. The mechanisms of the neurovascular coupling between underlying synaptic activity and the BOLD responses remain the subject of intensive current investigations (Logothetis, 2002; Smith et al., 2002; Ureshi et al., 2004; Stefanovic et al., 2006; Uludag et al., 2009). It is changes in blood flow and blood volume which lead to changes in deoxyhemoglobin levels, which are the basis for generating BOLD fMRI. Therefore, vascular effects can limit and effect the interpretation of BOLD fMRI.

Also, it is well known that the large vessels on the surface of the brain can lead to BOLD fMRI activation at sites remote to where the actual neuronal activation is (Ugurbil et al., 2003; Polimeni et al., 2010). Imprecise spatial coupling between neuronal activity and the physiological and metabolic events yielding the functional BOLD images has been reported, indicating that the BOLD response may extend beyond the locus of neuronal firing (Disbrow et al., 2000; Kim et al., 2004). The vascular response to neuronal activity may extend over several millimeters due to the propagation of deoxyhemoglobin changes in the vasculature as blood flows downstream to venous vessels, including the large surface draining veins distant from the site of neuronal activation. This is clearly seen in the high resolution fMRI maps obtained here where the large draining vein can be always seen on the surface of the

brain consistent with other reports at 11.7 T (Silva and Koretsky, 2002; Keilholz et al., 2006). It has been demonstrated that spin-echo BOLD at high fields is expected to reduce the artifacts associated with large vessels (Zhao et al., 2004; Parkers et al., 2005). Despite the expectation of reduction in vascular effects it is clear they can still be prominent under the imaging parameters used in this study. As can be seen in Fig. 2A, vessel contamination from the draining vein can still be detected under the conditions used, probably due to significant T_2^* weighting during the acquisition time of the EPI readout (Keilholz et al., 2005). To avoid large surface vessel effects care was taken to analyze data from deeper cortical tissue. However, it is still possible that the minor components detected are due to non-specific vascular effects from the neighboring activated regions.

To begin to address the issue of whether the minor component is neuronal or vascular in origin, CBV weighted fMRI was performed. There is evidence that CBV weighted fMRI is less affected by vascular artifacts due to the vasodilation primarily occurring in capillaries in close proximity to the neuronal activation (Mandeville et al., 1998; Keilholz et al., 2006; Zhao et al., 2006; Fukuda et al., 2006; Kim et al., 2008). Evidence for this is that the large draining vein is not detected using CBV weighted fMRI in the rodent somatosensory cortex (Keilholz et al., 2006) and that columns in the cat visual cortex are better mapped with CBV weighted fMRI than BOLD fMRI (Fukuda et al., 2006). The CBV weighted fMRI data was consistent with the BOLD fMRI data. Two spatial components could be detected and the border positions of the major and minor components obtained from CBV weighted fMRI and BOLD fMRI were in excellent agreement. These results lend some support to the notion that the minor components of the BOLD fMRI might be due to underlying neuronal activity rather than vascular artifacts from the neighboring regions. However, it is still not clear whether penetrating venules could contribute to CBV weighted fMRI in deep cortex.

It has been hypothesized in previous work that the increase in the extent of activation peripheral to major BOLD signals might reflect sub-threshold synaptic activity (Saad et al., 2003; Lauritzen, 2005). In these studies no comparison of the extent of activation with the underlying anatomy was made nor were the boundaries of these affects quantified. Here we demonstrate that the minor BOLD and CBV fMRI components extend well into the neighboring representation and therefore there is a possibility that they may represent neuronal communication between the two areas. Recently, the spatiotemporal patterns of electrical activity in the cortex were measured with voltage-sensitive fluorescent dyes (Orbach et al., 1985). It was shown that as measurements moved from the center of the region of maximal depolarization (excitation), the strength of hyperpolarization (interpreted as inhibitory activity) relative to the depolarization increased resulting in surround hyperpolarization at the periphery of the activation center (Derkikman et al., 2003). In another recent work it was indicated that the peripheral hyperpolarization is correlated with a decrease in oxygenation and concurrent arteriolar vasoconstriction (Devor et al., 2007). This predicts that there should be decreased BOLD fMRI in the area surrounding the active area. Both works relied on optical techniques that were restricted to the surface of the brain. Due to draining vein artifacts in this study we did not analyze the functional data close to the surface, and therefore we only showed that there are significant minor components in BOLD fMRI signal at the boundary of an active area in the deeper cortical regions. There was no evidence for significant decreases in BOLD signal and CBV weighted fMRI signal

anywhere through the cortical thickness. It has been shown that increased inhibition due to increased activity of interneurons can cause vasodilation, increases in blood flow and increases in fMRI (Caesar et al., 2003; Hamel, 2004; Pelled et al., 2009). Therefore, it can be suggested that the minor components of the BOLD signal may be due to increased inhibition consistent with the voltage sensitive dye imaging. Interestingly, for an induced cortical plasticity in adult rats we were able to observe an expansion of the forepaw representation (mapped by the boundary of the major component) into the cortical area corresponding to the hindpaw. The new border coincided with the border position of the minor component in the forepaw representation prior to plasticity. The denervation was performed in adult rats so that no structural/neuroarchitectural changes were associated with the plasticity (Wong-Riley and Welt, 1980). The capacity for functional plasticity observed by means of fMRI may be indicative of the unmasking of existing neuronal connections, which are normally not expressed (e.g. disruption of the local inhibitory interactions could produce this expansion). This is an intriguing result that could help arguing that there is some neuronal significance to the minor border component. Future work of directly measuring the activity from deep cortical layers at positions coinciding with the minor components of the BOLD would be necessary to enable determination of whether and what types of electrical activity may be responsible for the minor components detected.

The use of fMRI to quantitatively map the border positions of somatosensory representations should be very useful for studying plasticity, learning, and assessing recovery of function after damage (Karni et al., 1995; Kim et al., 2003; Taskin et al., 2006; Pelled et al., 2007; Pelled et al., 2009; Sydecum et al., 2009; van der Linden et al., 2009; Yu et al., 2010; Pawela et al., 2010; Wu et al., 2011; Petit and Wu, 2011). A major advantage of using BOLD fMRI for such studies would be the ability to study individual animals longitudinally. Specifically, studies of the changes in the functional boundaries using BOLD fMRI should further studies about the mechanism of neuronal reorganizations (Godde et al., 1996; McCandlish et al., 1996; Melzer et al., 1998; Godde et al., 2002; Calford, 2002). Furthermore, future clarifications of the spatial coupling between the neuronal activity and the physiological phenomena underlying the fMRI BOLD should help advance the understanding of the neuronal basis of fMRI. Finally, it will be interesting to extend the analysis performed here to the human brain to see if multiple spatial components along the borders of BOLD fMRI can be found and used to quantitate the boundaries of activation.

5. Conclusions

It has been demonstrated that sufficient signal averaging of very high-resolution BOLD fMRI maps in rats significantly improves the spatial stability of the BOLD signal. Under these conditions the BOLD fMRI signal at the boundaries of the maps was shown to have two spatial components. The major components enable mapping of the boundary between the forepaw and hindpaw that agrees with the histologically determined boundary. The minor component has about 30% of the amplitude of the major component. The boundaries of the minor component extend significantly into the neighboring regions.

The origins for the minor components are not clear and could be either of vascular or neuronal nature. This should be a subject of further investigation. An indication that the

minor component represents some form of underlying neuronal activity comes from the fact that CBV weighted fMRI gave similar results to BOLD fMRI. Quantitative determination of boundaries of neuronal representations from BOLD fMRI should be very useful for studies of plasticity and for helping to understand the neuronal basis of fMRI.

Acknowledgments

The authors would like to thank Nadia Bouraoud for animal preparation and physiology. This work was supported by the intramural research program of NINDS, NIH.

References

- Ajima A, Tanaka S. Spatial patterns of excitation and inhibition evoked by lateral connectivity in layer 2/3 of rat barrel cortex. *Cereb Cortex*. 2006; 16:1202–11. [PubMed: 16237202]
- Barbier EL, Marrett S, Danek A, Vortmeyer A, van Gelderen P, Duyn J, Bandettini P, Grafman J, Koretsky AP. Imaging cortical anatomy by high-resolution MR at 3.0T: detection of the stripe of Gennari in visual area 17. *Magn Reson Med*. 2002; 48:735–738. [PubMed: 12353293]
- Berwick J, Redgrave P, Jones M, Hewson-Stoate N, Martindale J, Johnston D, Mayhew JEW. Integration of neural responses originating from different regions of the cortical somatosensory map. *Brain Research*. 2004; 1030:284–293. [PubMed: 15571677]
- Bock C, Krep H, Brinker G, Hoehn-Berlage M. Brainmapping of α -chloralose anesthetized rats with T₂*-weighted imaging: distinction between the representation of the forepaw and hindpaw in the somatosensory cortex. *NMR Biomed*. 1998; 11:115–119. [PubMed: 9699494]
- Bock N, Kocharyan A, Liu JV, Silva AC. Visualizing the entire cortical myelination patterns in marmosets with magnetic resonance imaging. *J Neurosci Methods*. 2009; 185:15–22. [PubMed: 19737577]
- Caesar K, Thomsen K, Lauritzen M. Dissociation of spikes, synaptic activity, and activity-dependent increments in rat cerebellar blood flow by tonic synaptic inhibition. *Proc Natl Acad Sci USA*. 2003; 100:16000–16005. [PubMed: 14673091]
- Calford MB. Dynamic representational plasticity in sensory cortex. *Neuroscience*. 2002; 111:709–738. [PubMed: 12031401]
- Chapin JK, Lin C-S. Mapping the body representation in the SI cortex of anesthetized and awake rats. *J Comp Neurol*. 1984; 229:199–213. [PubMed: 6438190]
- Chapin JK, Sadeq M, Guise JLU. Corticocortical connections within the primary somatosensory cortex of the rat. *J Comp Neurol*. 1987; 263:326–346. [PubMed: 2822774]
- Chen NK, Oshio K, Panych LP. Application of k-space energy spectrum analysis to susceptibility field mapping and distortion correction in gradient-echo EPI. *NeuroImage*. 2006; 31:609–622. [PubMed: 16480898]
- Chen Z, Shen J. Single-shot echo-planar functional magnetic resonance imaging of representations of the fore- and hindpaws in the somatosensory cortex of rats using an 11.7 T microimager. *Journal of Neuroscience Methods*. 2006; 151:268–275. [PubMed: 16168491]
- Dawson DR, Killackey HP. The organization and mutability of the forepaw and hindpaw representations in the somatosensory cortex of the neonatal rat. *J Comp Neurol*. 1987; 256:246–256. [PubMed: 3558880]
- Derkikman D, Hildesheim R, Ahissar E, Arieli A, Grinvald A. Imaging spatiotemporal dynamics of surround inhibition in the barrels somatosensory cortex. *J Neurosci*. 2003; 23:3100–3105. [PubMed: 12716915]
- Devor A, Tian P, Nishimura N, Teng IC, Hillman EMC, Narayanan SN, Ulbert I, Boas DA, Kleinfeld D, Dale AM. Suppressed neuronal activity and concurrent arteriolar vasoconstriction may explain negative blood oxygenation level-dependent signal. *J Neurosci*. 2007; 27:4452–4459. [PubMed: 17442830]

- Disbrow EA, Slutsky DA, Roberts TPL, Krubitzer LA. Functional MRI at 1.5 Tesla: a comparison of the blood oxygenation level-dependent signal and electrophysiology. *Proceedings of the National Academy of Sciences of the United States of America*. 2000; 97:9718–9723. [PubMed: 10931954]
- Duong TQ, Kim DS, Ugurbil K, Kim S-G. Localized cerebral blood flow response at submillimeter columnar resolution. *Proc Natl Acad Sci USA*. 2001; 98:10904–10909. [PubMed: 11526212]
- Duyn JF, van Gelderen P, Li T-Q, de Zwart JA, Koretsky AP, Fukunaga M. High-field MRI of brain cortical substructure based on signal phase. *Proc Natl Acad Sci USA*. 2007; 104:11796–11801. [PubMed: 17586684]
- Engel SA, Glover GH, Wandell BA. Retinotopic organization in human visual cortex and the spatial precision of functional MRI. *Cerebral Cortex*. 1997; 7:181–192. [PubMed: 9087826]
- Fukuda M, Moon C-H, Wang P, Kim S-G. Mapping iso-orientation columns by contrast agent-enhanced functional magnetic resonance imaging: reproducibility, specificity, and evaluation by optical imaging of intrinsic signal. *J Neurosci*. 2006; 26:11821–11832. [PubMed: 17108155]
- Godde B, Berkefeld T, David-Jurgens M, Dinse HR. Age-related changes in primary somatosensory cortex of rats: evidence for parallel degenerative and plastic-adaptive processes. *Neuroscience and Biobehavioral Reviews*. 2002; 26:743–752. [PubMed: 12470685]
- Godde B, Spengler F, Dinse HR. Associative pairing of tactile stimulation induces somatosensory cortical reorganization in rats and humans. *Neuroreport*. 1996; 20:281–5. [PubMed: 9051796]
- Goloshevsky AG, Silva AC, Dodd SJ, Koretsky AP. BOLD fMRI and Somatosensory Evoked Potentials Are Well Correlated Over a Broad Range of Frequency Content of Somatosensory Stimulation of the Rat Forepaw. *Brain Res*. 2008; 1195:67–76. [PubMed: 18206862]
- Gruetter R. Automatic, localized in Vivo adjustment of all first- and second-order shim coils. *Magn Reson Med*. 1993; 29:804–811. [PubMed: 8350724]
- Hamel E. Cholinergic modulation of the cortical microvascular bed. *Prog Brain Res*. 2004; 145:171–178. [PubMed: 14650915]
- Hevner RF, Liu S, Wong-Riley MTT. A metabolic map of cytochrome oxidase in the rat brain: histochemical, densitometric and biochemical studies. *Neurosci*. 1995; 65:313–342.
- Hinds O, Polimeni JR, Rajendran N, Balasubramanian M, Amunts K, Zilles K, Schwarz EL, Fischl B, Triantafyllou C. Locating the functional and anatomical boundaries of human primary visual cortex. *NeuroImage*. 2009; 46:915–922. [PubMed: 19328238]
- Huettel SA, McCarthy G. The effects of single-trial averaging upon the spatial extent of fMRI activation. *Neuroreport*. 2001; 12:2411–2416. [PubMed: 11496120]
- Huettel, SA.; Song, AW.; McCarthy, G. *Functional magnetic resonance imaging*. Sinauer Associates, Inc; Sunderland, MA: 2004.
- Jin T, Kim SG. Cortical layer dependent dynamic blood oxygenation, cerebral blood flow, and cerebral blood volume responses during visual stimulation. *NeuroImage*. 2008; 43:1–9. [PubMed: 18655837]
- Karni A, Meyer G, Jezzard P, Adams MM, Turner R, Ungerleider L. Functional MRI evidence for adult motor cortex plasticity during motor skill learning. *Nature*. 1995; 377:155–158. [PubMed: 7675082]
- Keilholz SD, Silva AC, Dyun J, Koretsky AP. The contribution of T₂* to spin-echo EPI: implications for high-field fMRI studies. *Proc Intl Soc Mag Reson Med*. 2005; 13:32.
- Keilholz SD, Silva AC, Raman M, Merkle H, Koretsky AP. BOLD and CBV-weighted functional magnetic resonance imaging of the rat somatosensory system. *Magn Reson Med*. 2006; 55:316–24. [PubMed: 16372281]
- Kim D-S, Duong TQ, Kim S-G. High-resolution mapping of iso-orientation columns by fMRI. *Nat Neurosci*. 2000; 3:164–169. [PubMed: 10649572]
- Kim DS, Ronen I, Olman C, Kim SG, Ugurbil K, Toth LJ. Spatial relationship between neuronal activity and BOLD functional MRI. *Neuroimage*. 2004; 21:876–885. [PubMed: 15006654]
- Kim SG, Fukuda M. Lessons from fMRI about mapping cortical columns. *The Neuroscientist*. 2008; 14:287–299. [PubMed: 17989170]
- Kim YH, Jang SH, Chang Y, Byun WM, Son S, Ahn SH. Bilateral primary sensori-motor cortex activation of post-stroke mirror movements: an fMRI study. *Neuroreport*. 2003; 14:1329–1332. [PubMed: 12876467]

- Koopmans PJ, Barth M, Norris DG. Layer specific BOLD activation in human V1. *Human Brain Map.* 2010; 31:1297–1304.
- Land PW, Simons DJ. Cytochrome oxidase staining in the rat SmI Barrel Cortex. *J Comp Neurol.* 1985; 238:225–235. [PubMed: 2413086]
- Lauritzen M. Reading vascular changes in brain imaging: is dendritic calcium the key? *Nat Rev Neurosci.* 2005; 6:77–85. [PubMed: 15611729]
- Logothetis NK. The neuronal basis of the blood-oxygen-level-dependent functional magnetic resonance imaging signal. *Phil Trans R Soc Lond B.* 2002; 357:1003–1037. [PubMed: 12217171]
- Mandeville JB, Marota JJA, Kosofsky BE, Keltner JR, Weissleder R, Rosen BR, Weisskoff RM. Dynamic functional imaging of relative cerebral blood volume during rat forepaw stimulation. *Magn Reson Med.* 1998; 39:615–624. [PubMed: 9543424]
- McCandlish CA, Li CX, Waters RS, Howard EM. Digit removal leads to discrepancies between the structural and functional organization of the forepaw barrel subfield in layer IV of rat primary somatosensory cortex. *Exp Brain Res.* 1996; 108:417–426. [PubMed: 8801121]
- Melzer P, Smith CB. Plasticity of cerebral metabolic whisker maps in adult mice after whisker follicle removal – I. Modifications in barrel cortex coincide with reorganization of follicular innervation. *Neuroscience.* 1998; 83:27–41. [PubMed: 9466397]
- Ogawa S, Lee TM, Stepnoski R, Chen W, Zhu XH, Ugurbil K. An approach to probe some neural systems interaction by functional MRI at neural time scale down to milliseconds. *Proc Natl Acad Sci USA.* 2000; 97:11026–11031. [PubMed: 11005873]
- Orbach HS, Cohen LB, Grinvald A. Optical mapping of electrical activity in rat somatosensory and visual cortex. *J Neurosci.* 1985; 23:1298–1309.
- Palmer JT, de Crespigny AJ, Williams SP, Busch E, van Bruggen N. High-Resolution mapping of discrete representational areas in rat somatosensory cortex using blood volume-dependent functional MRI. *NeuroImage.* 1999; 9:383–392. [PubMed: 10191167]
- Park JC, Ronen I, Toth LJ, Ugurbil K, Kim DS. Comparison of point spread functions of BOLD and ASL fMRI at an ultra-high magnetic field, 9.4T. *Proc Intl Soc Mag Reson Med.* 2004; 11:1014.
- Parkers LM, Schwarzbach JV, Bouts AA, Deckers RHR, Pullens P, Kerskens CM, Norris DG. Quantifying the spatial resolution of the gradient echo and spin echo BOLD response at 3 Tesla. *Magnetic Resonance in Medicine.* 2005; 54:1465–1472. [PubMed: 16276507]
- Pawela CP, Biswal BB, Hudetz AG, Li R, Jones SR, Cho YR, Matloub HS, Hyde JS. Interhemispheric neuroplasticity following limb deafferentiation detected by resting-state functional connectivity magnetic resonance imaging (fcMRI) and functional magnetic resonance imaging (fMRI). *NeuroImage.* 2010; 49:2467–2478. [PubMed: 19796693]
- Pelled G, Chuang KH, Dodd SJ, Koretsky AP. Functional MRI detection of bilateral cortical reorganization in the rodent brain following peripheral nerve deafferentation. *NeuroImage.* 2007; 37:262–273. [PubMed: 17544301]
- Pelled G, Bergstrom DA, Tierney PL, Conroy RS, Chuang KH, Yu D, Leopold DA, Walters JR, Koretsky AP. Ipsilateral cortical fMRI responses after peripheral nerve damage in rats reflect increased interneuron activity. *Proc Natl Acad Sci.* 2009; 106:14114–14119. [PubMed: 19666522]
- Petit, A.; Wu, CWH. Detecting Acute Cortical Layer-Specific Plasticity in Rat Model using high field fMRI: Part 2- a non-thresholded, raw data analysis study. *ISMRM;* 2011. abstract
- Polimeni JR, Fischl B, Greve DN, Wald LL. Laminar analysis of 7T BOLD using an imposed spatial activation pattern in human V1. *NeuroImage.* 2010; 52:1334–1346. [PubMed: 20460157]
- Saad ZS, Ropella KM, DeYoe EA, Bandettini PA. The spatial extent of the BOLD response. *NeuroImage.* 2003; 19:132–144. [PubMed: 12781733]
- Shmuel A, Yacoub E, Chaimow D, Logothetis NK, Ugurbil K. Spatio-temporal point-spread function of fMRI signal in human gray matter at 7 Tesla. *NeuroImage.* 2007; 35:539–552. [PubMed: 17306989]
- Silva AC, Koretsky AP. Laminar specificity of functional MRI onset times during somatosensory stimulation in rat. *Proc Natl Acad Sci USA.* 2002; 99:15182–15187. [PubMed: 12407177]
- Silva AC, Lee JH, Wu CW-H, Tucciarone J, Pelled G, Aoki I, Koretsky AP. Detection of cortical laminar architecture using manganese-enhanced MRI. *J Neurosci Methods.* 2008; 167:246–257. [PubMed: 17936913]

- Smith AJ, Blumenfeld H, Behar KL, Rothman DL, Shulman RG, Hyder F. Cerebral energetics and spiking frequency: the neurophysiological basis of fMRI. *Proc Natl Acad Sci USA*. 2002; 99:10765–10770. [PubMed: 12134056]
- Spenger C, Josephson A, Klason T, Hoehn M, Schwindt W, Ingvar M, Olson L. Functional MRI at 4.7 Tesla of the rat brain during electric stimulation of forepaw, hindpaw, or tail in single- and multislice experiments. *Experimental Neurology*. 2000; 166:246–253. [PubMed: 11085890]
- Stefanovic B, Schwindt W, Hoehn M, Silva AC. Functional uncoupling of hemodynamic from neuronal response by inhibition of neuronal nitric oxide synthase. *J Cereb Blood Flow Metab*. 2007; 27:741–754. [PubMed: 16883353]
- Strupp JP. Stimulate: A GUI based fMRI analysis software package. *NeuroImage*. 1996; 3:S607.
- Sydecum E, Baltes C, Ghosh A, Mueggler T, Schwab ME, Rudin M. Functional reorganization in rat somatosensory cortex assessed by fMRI: elastic image registration based on structural landmarks in fMRI images and application to spinal cord injured rats. *NeuroImage*. 2009; 44:1345–1354. [PubMed: 19015037]
- Taskin B, Jungehulsing GJ, Ruben J, Brunecker P, Krause T, Blankenburg F, Villringer A. Preserved responsiveness of secondary somatosensory cortex in patients with thalamic stroke. *Cereb Cortex*. 2006; 16:1431–1439. [PubMed: 16357339]
- Thomas CG, Harshman RA, Menon RS. Noise reduction in BOLD-based fMRI using component analysis. *NeuroImage*. 2002; 17:1521–1537. [PubMed: 12414291]
- Tucker TR, Katz LC. Recruitment of local inhibitory networks by horizontal connections in layer 2/3 of ferret visual cortex. *J Neurophysiol*. 2003; 89:501–512. [PubMed: 12522197]
- Ugurbil K, Toth L, Kim DS. How accurate is magnetic resonance imaging of brain function? *Trends Neurosci*. 2003; 26:108–114. [PubMed: 12536134]
- Uludag K, Muller-Bierl B, Ugurbil K. An integrative model for neuronal activity-induced signal changes for gradient and spin-echo functional imaging. *NeuroImage*. 2009; 48:150–165. [PubMed: 19481163]
- Ureshi M, Matsuura T, Kanno I. Stimulus frequency dependence of the linear relationship between local cerebral blood flow and field potential evoked by activation of rat somatosensory cortex. *Neurosci Res*. 2004; 48:147–153. [PubMed: 14741389]
- Van der Linden A, van Meir V, Boumans T, Poirier C, Balthazart J. MRI in small brains displaying extensive plasticity. *Trends Neurosci*. 2009; 32:257–266. [PubMed: 19307029]
- Wong-Riley MT, Welt C. Histochemical changes in cytochrome oxidase of cortical barrels alter vibrissal removal in neonatal and adult mice. *Proc Natl Acad Sci USA*. 1980; 77:2333–2337. [PubMed: 6246540]
- Wu, CWH.; Goloshevsky, A.; Koretsky, AP. Detecting Acute Cortical Plasticity in Rats using High Field fMRI: Part 1- fMRI Maps and Cytoarchitectonic Boundaries. ISMRM; 2011. abstract
- Yeo BTT, Sabuncu MR, Vercauteren T, Holt DJ, Amunts K, Zilles K, Golland P, Fischl B. Learning task-optimal registration cost-functions for localizing cytoarchitecture and function in the cerebral cortex. *IEEE Trans Med Imag*. 2010; 29:1424–1441.
- Yu X, Wang S, Chen DY, Dodd S, Goloshevsky A, Koretsky AP. 3D mapping of somatotopic reorganization with small animal functional MRI. *NeuroImage*. 2010; 49:1667–1676. [PubMed: 19770051]
- Zhao F, Wang P, Hendrich K, Ugurbil K, Kim SG. Cortical layer-dependent BOLD and CBV responses measured by spin-echo and gradient-echo fMRI: insights into hemodynamic regulation. *NeuroImage*. 2006; 30:1149–1160. [PubMed: 16414284]
- Zhao FQ, Wang P, Kim S-G. Cortical depth-dependent gradient-echo and spin-echo BOLD fMRI at 9.4 T. *Magn Reson Med*. 2004; 51:518–524. [PubMed: 15004793]

Research highlights

- Spatial distribution of BOLD fMRI maps was studied for rat limbs.
- Signal distribution over the extent of fMRI maps was fit with 2 spatial components.
- Boundaries of BOLD fMRI maps were determined and compared to histological slices.
- Cortical plasticity in adult rat brain was studied after nerve deafferentiation.

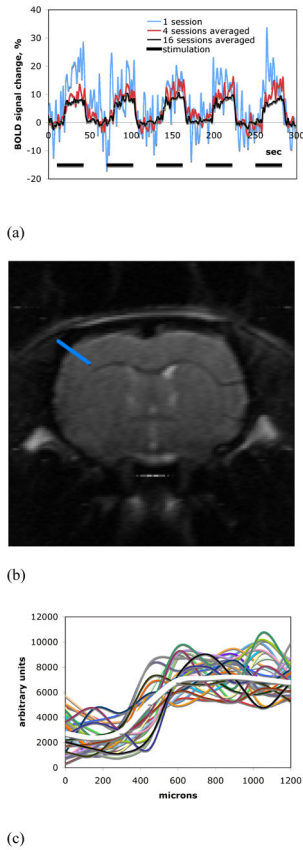
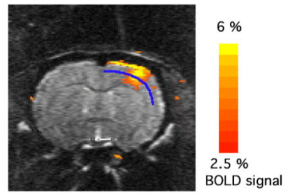
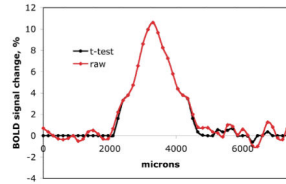


Fig. 1.

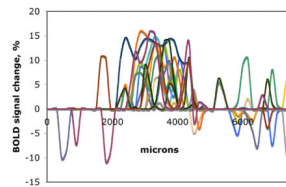
(A) Representative time courses of the observed BOLD fMRI signals. SNR of the fMRI response improves with the increased number of averages. (B) A representative high-resolution (150 μm , in-plane) anatomical spin-echo EPI image obtained after averaging of thirty-three fMRI sessions from a single animal. (C) A magnitude profile of the averaged anatomical image (white thick curve) and magnitude profiles of the single sessions (multicolored thin curves) used for averaging. All signal profiles correspond to the same ROI across the edge of the cortex as shown in (B).



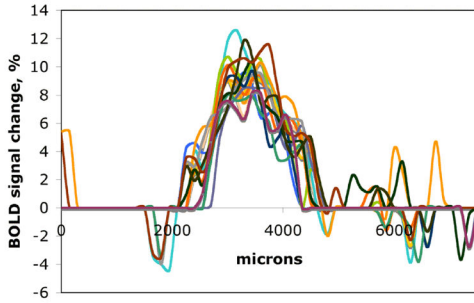
(a)



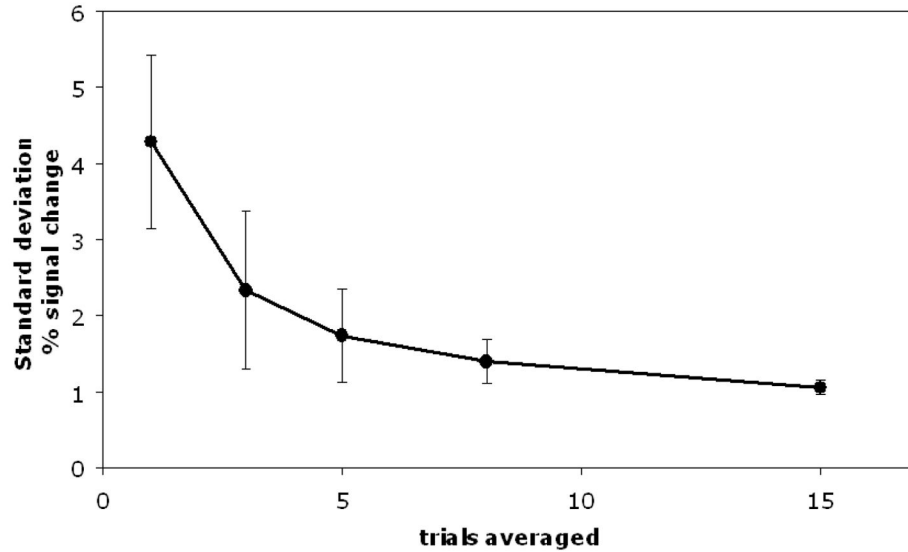
(b)



(c)



(d)



(e)

Fig. 2.

(A) An averaged BOLD activation map of forepaw representation overlaid upon an averaged anatomical image. Twenty fMRI sessions, obtained from a single animal with the in-plane resolution of 150 μm (multi-slice SE EPI), were averaged for the shown image and the activation map. (B) Comparison of BOLD activation map profiles from the ROI shown in (A) corresponding to the functional averaged data unprocessed (diamonds, red) and after t-test (circles, black).

Dependence of the activation profiles upon the number of averages: (C) 15 randomly sampled fMRI sessions and (D) a series of 15 averages of 8 randomly sampled sessions. All the profiles are from the same ROI shown in (A). As more fMRI sessions are averaged, stability of the activation profile increases.

(E) Standard deviation of the BOLD signal at the border of activation area versus the number of averaged trials.

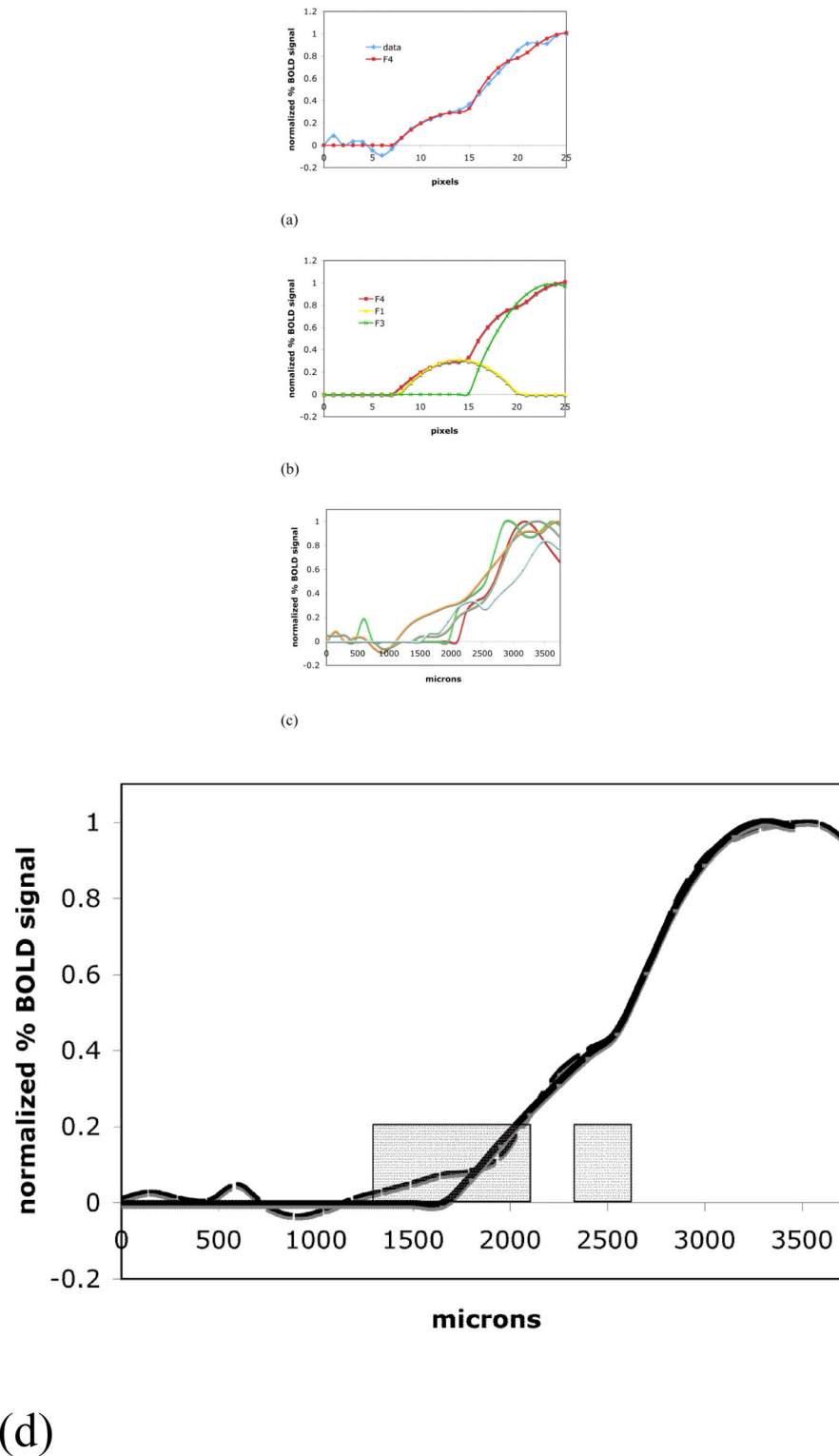
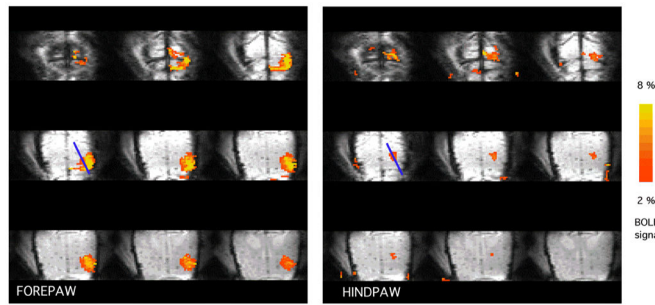


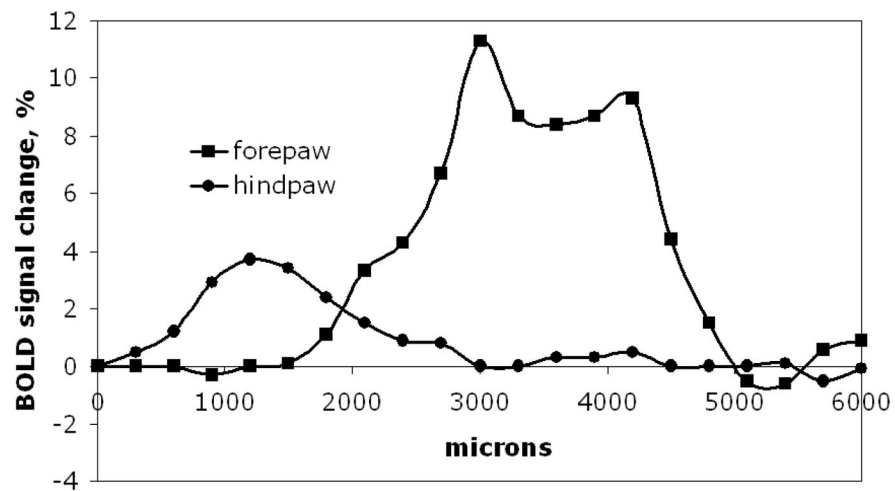
Fig. 3. (A) Either half of a typical symmetrical activation profile can be well fitted by a combination (shown in (B)) of two parabolic-shaped curves. The fit curves F_4 , F_1 and F_3

represent the equations (1), (2) and (4). The differentiation of the lower and higher BOLD signal in an activation profile can be measured by the points where the representative parabolic-shaped curves cross-section the abscissa.

(C) An area of lower BOLD signal bordered the area of major BOLD signal for all five animals used in the high-resolution experiments. (D) The high-resolution averaged activation profile (dashed line), its fit curve (thicker solid line) and the averaged $zero_{major}$ and $zero_{minor}$ points of the abscissa cross-section (mean \pm SD, grey boxes).

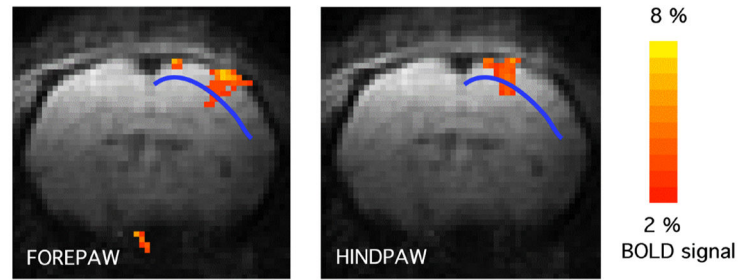


(a)

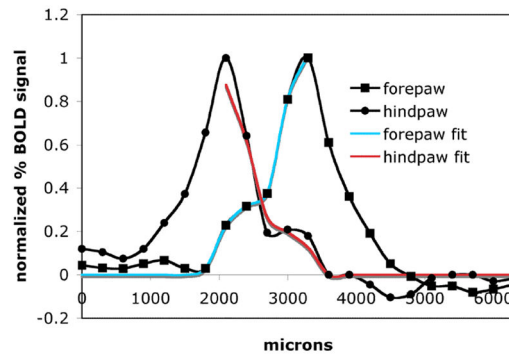


(b)

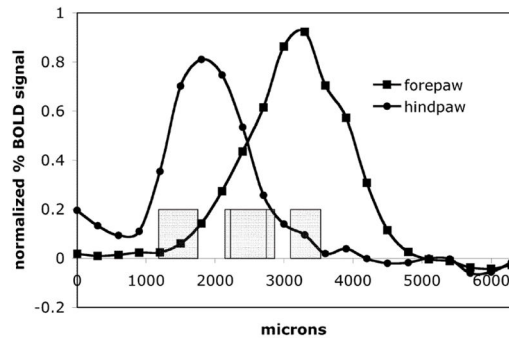
Fig. 4. (A) Representative averaged forepaw and hindpaw activation maps overlaid upon averaged anatomical images are shown in axial orientation. Thirteen fMRI sessions, separately obtained for each limb from a single animal with the isotropic resolution of 300 μm (3D GE EPI), were averaged for the shown images and the activation maps. (B) BOLD signal profiles from the activation maps of forepaw and hindpaw corresponding to the ROI shown in (A).



(a)



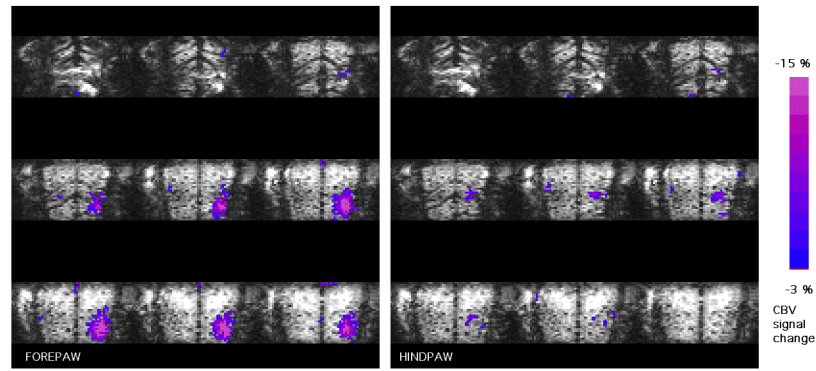
(b)



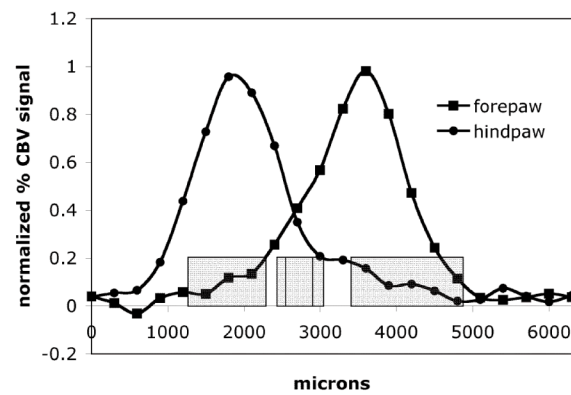
(c)

Fig. 5.

(A) Representative averaged activation maps of forepaw and hindpaw overlaid upon averaged anatomical images are shown in coronal orientation. (B) Normalized BOLD signal profiles of the forepaw and hindpaw representations and their fit curves corresponding to the same ROI shown in (A). The profiles and their fit curves exhibit a significant overlap between the representations. (C) Normalized BOLD signal profiles of forepaw and hindpaw averaged for five animals and the averaged $zero_{major}$ and $zero_{minor}$ points of the abscissa cross-section (mean \pm SD, grey boxes).



(a)



(b)

Fig. 6. (A) Representative averaged CBV activation maps of forepaw and hindpaw overlaid upon averaged anatomical images are shown in axial orientation. (B) Normalized CBV signal profiles of forepaw and hindpaw averaged for five animals and the averaged $zero_{major}$ and $zero_{minor}$ points of the abscissa cross-section (mean \pm SD, grey boxes).

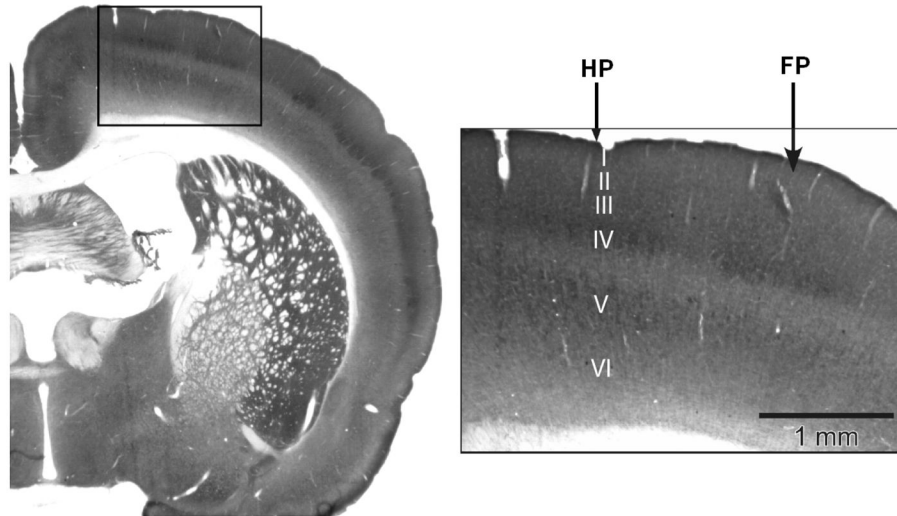
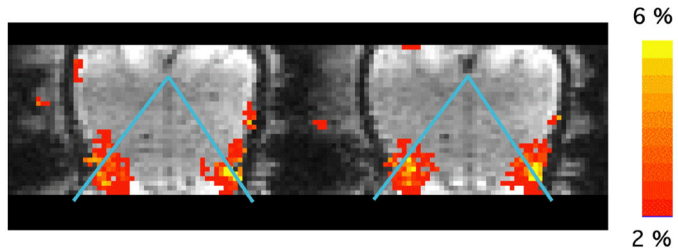
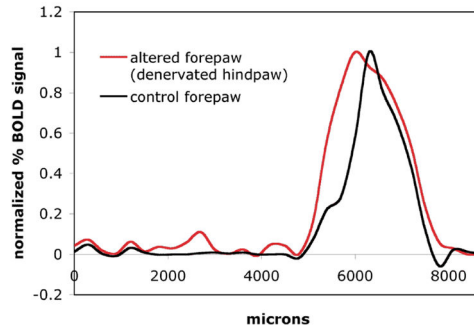


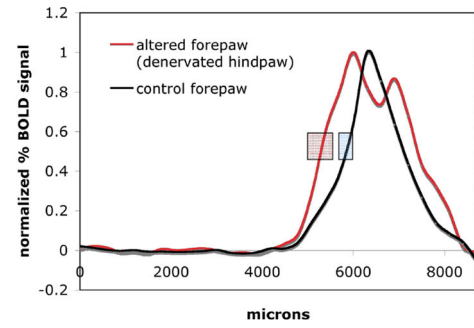
Fig. 7. A typical histochemically stained (cytochrome oxidase) slice of the rat brain. Arrows indicate the cytoarchitectural representations of forepaw and hindpaw, distinctively visible in the cortical layer IV (labeled).



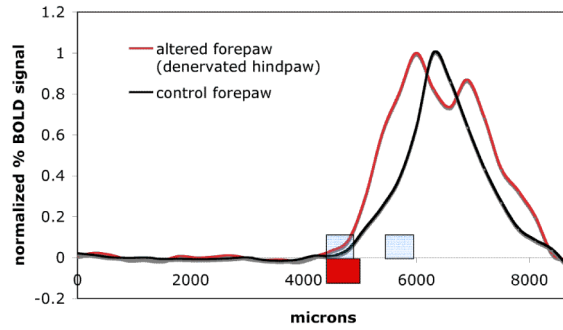
(a)



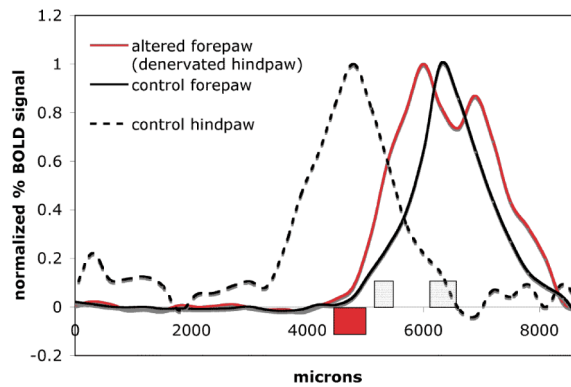
(b)



(c)



(d)



(e)

Fig. 8.

(A) fMRI map from a denervated animal showing activation of the normal forepaw cortex (right) and forepaw cortex on the side where the hindpaw was denervated (left). The blue lines indicate the line that profiles were derived from. (B) Difference shown between the forepaw BOLD signal intensity profiles on the unaffected side (black line) and the affected forepaw representation (red line) from a single representative animal. The expected expansion of the forepaw representation into the cortical area of the denervated hindpaw can be seen. (C) BOLD signal intensity profiles on the unaffected side (black line) and the affected forepaw representation (red line). The difference in position of the half-height point borders (averaged across the animals) of the major components of the map profiles indicates an expansion of the forepaw representation. The boxes represent the mean \pm one standard deviation in position. (D) Expansion of the forepaw cortical map representation into the hindpaw representation based on fitting. Boxes indicate the positions of the $zero_{major}$ and $zero_{minor}$ points of the abscissa cross-section (mean \pm SD) of control forepaw (blue boxes) and $zero_{major}$ of the altered forepaw (red box) shown superposed on the activation profiles (averaged across animals) of the corresponding fMRI representations. (E) Shown are the hindpaw representation from the control side (dotted line) and its averaged $zero_{major}$ and

zero_{minor} points (grey boxes). Also shown is the average forepaw representation to demonstrate that it grew well within the major border of the hindpaw representation.

Table 1

The summary of the fit cross-section $zero_{major}$ and $zero_{minor}$ abscissa values (described by the equations (6) and (7)), obtained from the forepaw activation maps with the in-plane resolution of 150 μm . The abscissa values in microns were counted from the midline of the brain along the ROI selection

animal	1	2	3	4	5	averaged
$zero_{minor}$	1715	1723	1054	1950	2100	1709 \pm 400
$zero_{major}$	2591	2532	2250	2518	2534	2485 \pm 134

Table 2

The summary of the fit cross-section $zero_{major}$ and $zero_{minor}$ abscissa values (described by the equations (6) and (7)), obtained from the three-dimensional BOLD activation maps of forepaw and hindpaw with the isotropic resolution of 300 μm . The values were used to quantify the overlap of the forepaw and hindpaw BOLD fMRI representations. The abscissa values in microns were counted from the midline of the brain along the ROI selection

animal	1	2	3	4	5	averaged	
forepaw	$zero_{minor}$	1613	1133	1172	1631	1765	1463 ± 289
	$zero_{major}$	2255	2245	2185	2820	2669	2435 ± 289
hindpaw	$zero_{major}$	2461	2235	2456	3035	2749	2587 ± 310
	$zero_{minor}$	3178	3487	2997	3473	3534	3334 ± 235

Table 3

The summary of the fit cross-section $zero_{major}$ and $zero_{minor}$ abscissa values (described by the equations (6) and (7)), obtained from the three-dimensional CBV activation maps of forepaw and hindpaw with the isotropic resolution of 300 μm . The values were used to quantify the overlap of the forepaw and hindpaw CBV fMRI representations. The abscissa values in microns were counted from the midline of the brain along the ROI selection

animal	1	2	3	4	5	averaged	
forepaw	$zero_{minor}$	2013	1393	1203	2401	1973	1797 ± 490
	$zero_{major}$	3054	2781	2280	2909	2799	2765 ± 292
hindpaw	$zero_{major}$	2608	2906	2588	2810	2688	2720 ± 136
	$zero_{minor}$	3900	3993	4619	5165	3054	4146 ± 797

Table 4

The summary of the borders between the somatosensory representations of forepaw and hindpaw obtained from the scored photoimages of the histochemically stained (CO) brain sections. The border values in microns were measured from the midline of the brain along the ROI selection line

animal	1	2	3	4	averaged
forepaw left border	2841	2883	2930	2892	2887 ± 37
hindpaw right border	2470	2536	2611	2552	2542 ± 58

Table 5

The summary of the fit cross-section $zero_{major}$ and $zero_{minor}$ abscissa values (described by the equations (6) and (7) and averaged across the animals) and the abscissa values of the half-height of the major profile component (averaged across the animals) corresponding to the somatosensory representations of the control forepaw, altered forepaw and control hindpaw

	$zero_{major}, \mu\text{m}$	$zero_{minor} \mu\text{m}$	half-height, μm
control forepaw	5743 ± 195	4696 ± 233	5856 ± 105
altered forepaw	4768 ± 273	-	5296 ± 278
control hindpaw	5351 ± 139	6404 ± 214	-